J Fusion Energ (2008) 27:91–95
DOI 10.1007/s10894-007-9113-2

ORIGINAL PAPER

Energy Confinement Scaling Predictions for the Stabilized Tandem Mirror

J. Pratt · W. Horton · H. L. Berk

Published online: 21 July 2007

Abstract The absence of toroidal curvature and the relatively weak internal parallel currents in a tandem mirror gives the system favorable stability and transport properties. GAMMA-10 experiments demonstrate that sheared plasma rotation suppresses turbulent radial losses through control of the radial potential profiles. Recent achievements of the GAMMA-10 include 3 keV ion confinement potentials and $T_e \geq 800$ eV. Total energy confinement times for the GAMMA-10 experiment exceed by an order of magnitude the corresponding empirical confinement times in toroidal devices. At the temperatures achieved in the GAMMA-10, the end loss rate $\tau_p \simeq 100$ ms so that radial losses determine τ_E, as intended in tandem mirror reactor designs. Drift-wave results on radial confinement times developed using Bohm, gyro-Bohm, and electron temperature gradient (ETG) scalings imply that the tandem mirror has a qualitatively different form of drift-wave radial transport from that in toroidal devices. Drift-wave eigenmodes for the GAMMA-10 are analyzed for the fluctuating electrostatic potential and magnetic perturbations.

Keywords Tandem mirror · Fusion power · Burning plasmas · Magnetic confinement

Characterization of Tandem Mirror Systems

Tandem mirror plasmas are guarded by strong, radially sheared flow (for transverse confinement like H-mode or ITB in tokamaks) and high plugging potentials (in the axial direction). The tandem mirror magnetic-fusion confinement system is a long cylindrical solenoid bounded by a set of mirror cells; these mirror cells are designed to establish a positive electrostatic confinement potential ϕ_c and a thermal barrier region that produces a dip ϕ_b in the electrostatic potential. This confinement potential ϕ_c reflects small pitch-angle ions back toward the central cell whereas ϕ_b reflects the electrons. In contrast to the first tandem mirror device, TMX at Lawrence Livermore National Laboratory, the GAMMA-10 device is designed so that the electrons encounter the thermal barrier first and the ions encounter the ion confinement potential farther from the central cell. Two MHD-stabilizing quadrupole cells, maintained with neutral beam injected ions, sit immediately outside the central cell before the barrier and plug cells. Table 1 gives typical parameters of the GAMMA-10 system.

Figure 1 shows the on-axis magnetic field that describes the geometry of the GAMMA-10. Pictured in Fig. 1 is the simple analytical model we have constructed to match the data provided by the GAMMA-10 team. Based upon the average relative variance $(1/N)\sum_1^N (x_i - y_i)^2/\sigma_y^2$, our model matches the variation of the data with 99% accuracy.

The GAMMA-10 is axisymmetric except for the anchor cell where a quadrupole magnetic field is applied to insure MHD stability. Currently, open systems are being designed that are entirely axisymmetric, are MHD stable as a result of plasma pressure from the diverter region, and possess a fan shaped magnetic field on the outside of the plug barrier cells [1].

The absence of toroidal curvature in open systems gives them a fundamental advantage over toroidal systems that must contend with both large scale MHD instabilities and micro-scale drift-wave instabilities triggered by the plasma accelerating outward. Ballooning instabilities and other

J. Pratt (✉) · W. Horton · H. L. Berk
University of Texas at Austin, IFS, Austin, TX, USA
e-mail: jpratt@physics.utexas.edu

Table 1 Machine parameters

Parameter	G10 Dec. 2006	KSTM-FR [4]
a	0.18 m	1.5 m
L	6 m	30 m
n_c	10^{19} m^{-3}	10^{20} m^{-3}
n_p/n_c	0.1	7
T_e	750 eV	60 keV
T_i	6.5 keV (perp) 2.5 keV (par)	15 keV
B_{cc}	0.405 T	3 T
B_{plug}	0.49 T	18 T
R_m	5.2	9

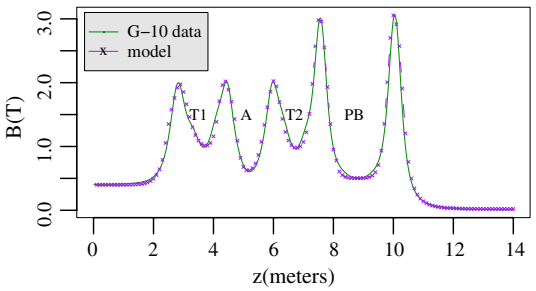

Fig. 1 Profiles of the axial B in the right-hand side of the GAMMA-10. Initials mark regions set up by the mirror coil configurations: transition region 1, anchor, transition region 2, and the plug-barrier region

large radially extended structures that arise from this toroidal acceleration $g_{tor} = c_s^2/R_c = 10^{11}$ m/s^2 are problems that must be addressed by keeping the plasma pressure low and its radial gradient below both the ideal beta limit and the limit for ballooning interchange modes [2]. Micro-scale turbulent instabilities remain a significant problem in tokamaks. The GAMMA-10 anchor cells have been crafted to limit these instabilities [3].

In contrast to toroidal devices, mirror systems have simpler particle orbits and better exterior access that allows control of the E_r shear. Open systems allow external control of the plasma radial field $E_r(r,t)$ profile. This is accomplished either through direct end-plate control or with the use of localized electron cyclotron heating power that increases the intrinsic ambipolar potential $\Delta\phi_{amb}(r) = \Phi_{plasma} - \Phi_{wall} \approx \Delta T_e \ln\sqrt{m_i/m_e} = 3.76\Delta T_e$ along the $\omega_{RF} = \omega_{ce}$ resonant surface [1]. The E_r profile is controlled by the ECH heating in the plug barrier plasmas with $P_{ECH}^{plug} \leq 380$ kW.

Radial and Axial Transport

For high temperature tandem mirror operation, the energy confinement time from radial transport, τ_E, dominates over the end loss transport. Comparisons of radial confinement times from theoretical drift-wave turbulence or from empirical databases (which can be used as conservative upper bounds on the theory) demonstrate this confinement time ordering. There are four standard empirical formulae derived from large international databases: (a) the L-mode tokamak confinement time, τ_E^{L97} [5], (b) the H-mode tokamak confinement time, τ_E^{H98} [6], (c) the international stellarator database formula from 1995 τ_E^{ISS95}, (d) the most recent stellarator database formula, τ_E^{ISS04} [7]. These four models were adapted to the geometry of a tandem mirror in Pratt and Horton [4]. Tokamak formulae originally involve the plasma current I_p but cover a limited range of safety factor $q = aB_T/RB_p$ values. To make the adaption to tandem mirrors a fixed q value ($q = 2$) was chosen to obtain the tokamak empirical energy confinement as a function of machine circumference $L = 2\,\pi\,R$, minor radius a, external magnetic field $B = B_T$. As a result, the tokamak scaling formulae and stellerator scaling formulae given in Table 2 are rendered in a comparable form; Table 3 gives the full set of predicted τ_E values derived from these formulae. Actually the value of q used is low enough that there will be $m/n = 1/1$ resonant surfaces in the tokamak that causes large slow sawtooth oscillations [8]. It is unclear that extrapolating the tokamak formulae that increase nearly linearly with plasma current I_p to such large plasma currents is within the domain of the ITER database. Table 3 also shows theoretical confinement times as well as ISS04 confinement time for the ITER reference parameters (R/a = 6.2/2.0, B_T = 5.3 T, $P_{external}$ = 40 MW, I_p = 15 mA).

Table 3 shows a consistent pattern of global radial energy confinement times. We argue that the evidence from the tandem mirrors and from general open systems demonstrates a large improvement over these formulae. We attribute the improved confinement to the different nature of the curvature and $\nabla \boldsymbol{B}$ drifts in the open and toroidal sys-

Table 2 Radial loss time scaling laws

$\tau_{L97} = 0.010$	$B^{0.99}$	$L^{0.93}$	$a^{1.86}$	$n^{0.4}$	$P^{-0.73}$
$\tau_{H98} = 0.067$	$B^{1.08}$	$L^{0.46}$	$a^{2.44}$	$n^{0.41}$	$P^{-0.69}$
$\tau_{ISS95} = 0.080$	$B^{0.83}$	$L^{0.65}$	$a^{2.21}$	$n^{0.51}$	$P^{-0.59}$
$\tau_{ISS04} = 0.103$	$B^{0.89}$	$L^{0.6}$	$a^{2.33}$	$n^{0.59}$	$P^{-0.64}$
$\tau_E^B = 0.042$	$B^{1/2}$	$L^{1/2}$	a^2	$n^{1/2}$	$P^{-1/2}$
$\tau_E^{gB} = 0.016$	$B^{0.8}$	$L^{0.6}$	$a^{2.4}$	$n^{0.6}$	$P^{-0.6}$
$\tau_E^{ETG} = 0.025$	–	$L^{0.33}$	$a^{2.66}$	n^1	$P^{-0.33}$

Table 3 Radial energy loss time for fusion machines

	G10 (ms)	NSTX (ms)	ITER (s)	KSTM (s)
τ_E^B	3.6	20.0	–	0.90
τ_E^{gB}	1.0	5.6	–	0.78
τ_E^{ETG}	0.7	20.0	–	1.1
τ_E^{L97}	2.0	4.6	2.72	.70
τ_E^{H98}	2.0	11.0	5.44	1.5
τ_E^{ISS95}	5.3	30	–	3.7
τ_E^{ISS04}	5.0	32	–	4.8

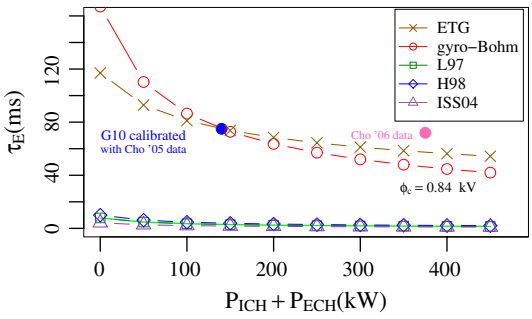

Fig. 2 Radial energy confinement times τ_E with dimensionless coefficient calibrated to match the data quoted in [16], 75 ms. In 2006 confinement reached 100 ms in the GAMMA-10; the GAMMA-10 shows an enhancement of more than a factor of 3 for the 2006 data over the equivalent sized toroidal systems. 2006 data for a similar discharge is 72 ms at 380 kW of power [17]. Depicted far below these theoretical confinement models are tokamak and stellerator confinement time scaling laws derived from large experimental databases

tems. The magnetic field curvature in an open system for a field-line close to the axis of the cylinder of radius $a(z) = r_0(B_0/B(z))^{1/2}$ is $1/R_c = -(\partial^2 a/\partial z^2) \leq \pm a/L_t^2$; neighboring regions of favorable ($R_c < 0$) and unfavorable ($R_c > 0$) curvature occur, separated by the transition scale length $L_t \ll L$. Thus the modes cannot balloon into the short unfavorable region L_t; favorable and unfavorable curvature regions tend to average on larger scales. In toroidal systems the unfavorable regions cover the entire outer half of the torus, giving rise to ballooning modes localized in regions of $g_{eff} = c_s^2/R$ where $R = R_c$ is the major radius of the torus. The most unstable eigenmode in the mirror system has an almost constant amplitude of the perturbed electrostatic potential $\phi_m(\boldsymbol{r}, t) = \phi_m(r/a, s/L) \exp i(m\theta - \omega t) + \text{c.c.}$ along the magnetic field. The higher order axial modes with $k_{||} = n\pi/L$ (n = 1,2,...) are kinetic shear-Alfven eigenmodes with positive, stable eigenvalues λ.

The Interchange Mode and Shear-Alfven Eigenmodes

The central cell plasma is maintained by symmetrically placed ICRF antennas at $z = \pm$ 2.5 m in the central cell. With total injected power P_{RF} = 170 kW, the steady state power balance (pb) gives $\tau_E = W/P_{RF} = 10^4\,\text{J}/170\,\text{kW} = 58.8\,\text{ms}$. We compare the effective thermal diffusivity with the toroidal ITG simulation value given, respectively, by

$$\chi_E^{pb} = a^2/4\tau_E = 0.28\,\text{m}^2/\text{s} \quad (1)$$

$$\chi_{gB}^{sim} = 1.7(\rho_i/a)(T_i/eB) \approx 10^3\,\text{m}^2/\text{s}. \quad (2)$$

We find that $\chi_E^{pb} \ll \chi_{gB}^{sim}$ from the standard ITG drift-wave turbulence model. The lowest-diffusivity model and most relevant theoretical model is the electromagnetic ETG formula [9] due to $\beta m_i/m_e \approx 294(\beta \simeq 0.16)$. The ETG formula is $\chi_{ETG}^e = (m_e/\beta_e m_i)(eT_e/eB) \approx 10\,\text{m/s}^2$. Thus, the radial diffusivity inferred from power balance in the GAMMA-10 is at least one order of magnitude lower than the standard drift-waves-theory formulae. In Fig. 2 we plot τ_E from the formulae for gyro-Bohm, L97, H98, and ISS04 as a function of the auxiliary power up to 500 kW.

Drift Alfven-Ballooning Interchange

Drift modes have $E_{||} \neq 0$ as opposed to MHD modes. For electron fluid motion parallel to $\boldsymbol{B}$

$$\frac{du_{||e}}{dt} = -\frac{e}{m_e}E_{||} - \frac{\nabla_{||}p_e}{m_e n_e} - \mu_e|\nabla_{||}| \quad (3)$$

where $u_{||e}$ gives the fluctuating parallel plasma current through $\delta j_{||} = -enu_{||}$, and $|\nabla_{||}|$ represents the absolute value of the wavenumber K in Fourier space. This leads to electron collisionless skin depth $\delta_e = c/\omega_{pe} \geq 0.0024\,\text{m}$, and sound radius $\rho_s = \sqrt{m_i T_e}/e\boldsymbol{B} \leq 0.1\,\text{cm}$. The hot ion gyroradius is $\rho_i \leq 1\,\text{cm}$. The kinetic Alfven wave dispersion relation is

$$\omega^2 = k_{||}^2 v_A^2 \left[\frac{1 + k_\perp^2(\rho_s^2 + \frac{3}{4}\rho_i^2)}{1 + k_\perp^2\delta_e^2}\right]. \quad (4)$$

There is a spectrum of global Alfven drift modes in the tandem mirror system. There are two drift-wave eigenmodes in the central cell, as sketched in Fig. 4. The axially symmetric eigenmode shown in Fig. 4 arises from the dispersion relations in Eq. 4 when the effects of $\omega_{*i} = (k_\theta/eBn)dp_i/dr$ and

$$\omega_{Di} = \frac{k_\theta T_i}{eB}\frac{d}{dr}\ln B = \omega_{\nabla B_v} - \frac{1}{2}\beta_i\omega_{*i} \quad (5)$$

are included. The wave rotates in the ion diamagnetic direction and evolves into the MHD-ballooning mode

instability when the ion pressure gradient is sufficiently high.

In the presence of strong sheared $\boldsymbol{E} \times \boldsymbol{B}$ rotation defined by $\Omega' = (d/dr)u_\theta/r$ where $u_\theta = -E_r(r)/B_{cc}$, the growth time is limited by the shearing time $1/\Omega'$ and simulations by Kim et al. [10] show an intermittent growth and decay of the instability. The dimensionless parameter governing the intermittency is $\Gamma_{MHD} = \gamma_{MHD}/r\Omega' \ln\sqrt{m_i/m_e}$ where γ_{MHD} is computed in the absence of sheared flows.

Alfven-MHD Eigenmodes

The eigenmode equation for $E_{||} = 0$ modes describes the $k_{||}$ spectrum of modes from

$$B\frac{\partial}{\partial z}\frac{k_\perp^2(z)}{B(z)}\frac{\partial\phi}{\partial z} = -\left[\frac{\rho\omega^2k^2}{B^2} + \frac{2k_\theta^2\kappa_r}{B^2}\frac{\partial p}{\partial r}\right]\phi \tag{6}$$

where $\kappa = (\hat{b}\cdot\nabla)\hat{b} = d^2a(z)/dz^2 = -1/R_c$. The lowest eigenmode may have negative $\omega^2 \simeq -p/(\rho R_c L_p)$ when the plasma beta is high enough. The condition on β for instability follows from a shooting code that calculates the slight localization in unfavorable curvature regions from Eq. 6. This critical beta limit is high—approaching unity for tandem mirrors—indicating its superior MHD stability. In this work we assume that the plasma pressure remains below this limit. Ryutov and Post give methods of enhancing the pressure limit by providing kinetic plasma flows and injection from the end regions into the last cell [11]. This is called the kinetically stabilized tandem mirror (KSTM). The eigenmode equation is

$$\frac{\partial^2\phi}{\partial z^2} = -\left[\omega(\omega-\omega_{*i})\frac{a^4}{v_A^2} - \frac{\gamma_{MHD}^2}{v_A^2}a^3\frac{d^2a}{dz^2}\right]\phi. \tag{7}$$

We solve Eq. 7 with a shooting code with two types of boundary conditions: (1) insulating end walls $d\phi/dz(\pm L) = 0$ and (2) conducting end walls $\phi(\pm L) = 0$. We vary L and the parameters of the problem. The upper graph in Fig. 3 shows the local growth rate γ_{MHD}^2 scaled by the Alfven velocity v_A^2 for 1 keV hydrogen plasma with $L_p = a = 0.18\,\text{m}$, $r_0 = 0.09\,\text{m}$, and $R_c = L_t^2/a$. The lower graph in Fig. 3 shows the lowest eigenmodes of Eq. 7 for the boundary conditions that correspond to insulating and conducting walls.

Electron Drift Waves and Shooting Eigenmode Results

In Fig. 4 we sketch the electron drift wave that follows from the conditions $\omega_{bi} \simeq k_{||}v_i < \omega_k < \omega_{be} < k_{||}v_e$. In the electron drift wave the condition on the axial wave number and wave frequency leads to the dominant electron response $\tilde{n} = n_e(e\tilde{\phi}/T_e)(1 - i\delta_k^e)$ where i δ_k^e is resonant

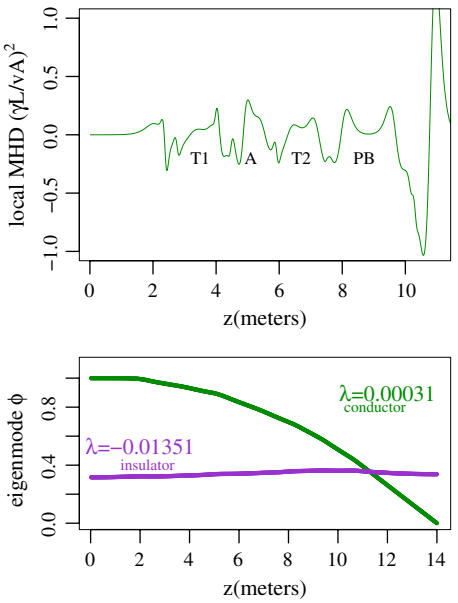

Fig. 3 (Above) The local γ_{MHD}^2 for the GAMMA-10 profile in Fig. 1. (Below) The lowest eigenvalues for the conducting end wall and the insulating end wall. Here we use L_t = 0.10 m

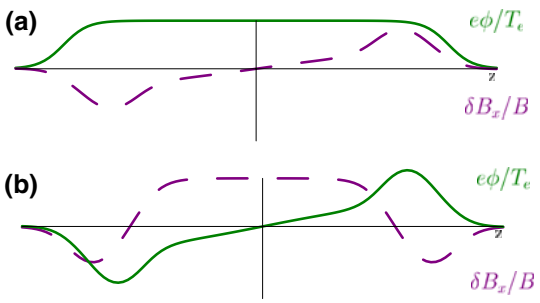

Fig. 4 (a) A sketch of the ion drift modes. (b) The electron drift modes

electron-wave response. In the presence of hot anisotropic ions ($T_{\perp,i} > 2T_{||,i} > T_e$) as in the central cell of the GAMMA-10, the wave growth is a function of the system parameters in Table 1.

The ion temperature gradient mode (ITG) in the long cylindrical geometry is in the regime where the gradient of the parallel temperature is dominant and the parallel ion Landau resonance $\omega = k_{||}v_{||}$ is the most important ion resonance. This regime is shown in Migliuolo [12] and Kim et al. [13] to have a weak growth rate that becomes small as $T_\perp$ increases. In a slab-like regime the radial gradient of the parallel ion temperature drives instabilities; in a toroidal system, the perpendicular ion temperature gradient drives the instability. Thus we expect the ITG and trapped ion mode to be weak in the GAMMA-10 device and readily stabilized by the E_r shear.

Conclusions

A review of the differences between the driving forces of instability and transport in the tandem mirror and toroidal magnetic confinement systems reveals several important advantages of open systems. Absence of a large uniform outward acceleration allows the cylindrical tandem mirror system to be MHD stable at high values of the dimensionless plasma pressure β. Micro-instabilities are weakened because of a high plasma β [14]. Local regions of magnetic-curvature oscillations ($\pm c_s^2 a/L_t^2$) in the transition regions, shown in Fig. 3, are averaged by fast axial Alfven wave propagation. The lowest axial eigenfunctions average the curvature over these regions reduce net unfavorable curvature over the total length through the last plug barrier end cell. We hypothesize that the radial transport in the tandem mirror system is intrinsically much lower than that in the corresponding toroidal system. The remaining low level drift waves are shown by Cho et al. to be controlled by the E_r shear [15].

Recent high ion and electron temperatures obtained in the GAMMA-10 device at relatively low injected RF power levels are used in both the empirical database energy confinement laws and the standard theoretical model confinement laws. The confinement results shown in Table 3 and Fig. 2 support the hypothesis that tandem mirrors are governed by new radial confinement laws. A database of high performance tandem mirror confinement discharges needs to be assembled.

Acknowledgement Work supported by the Department of Energy Grant DE-FG02-04ER5474.

References

1. I. Katanuma, Y. Sasagawa, Y. Tatematsu, Y. Nakashima, T. Cho, V. Pastukhov, Nucl. Fus. **46**, 608 (2006)
2. A.V. Anikeev, P.A. Bagryansky, P.P. Deichuli et al., Phys. Plasmas **4**, 347 (1997)
3. I. Katanuma, Y. Tatematsu, K. Ishii, T. Tamano, K. Yatsu, J. Phys. Soc. Japan **69**, 3244 (2000)
4. J. Pratt, W. Horton, Phys. Plasmas **13**, 042513-3 (2006)
5. S.M. Kaye, the ITER Confinement Database Working Group, Nucl. Fus. **37**, 1303 (1997)
6. G. Becker, Nucl. Fus., **44**, L26 (2004)
7. J.A. Rome, Stellarator News **92**, 280 (2004)
8. F. Porcelli, D. Boucher, M.N. Rosenbluth, Plasma Phys. Controlled Fus. **38**, 2163 (1996)
9. W. Horton Jr., Phys. Fluids **24**(7), 1272 (1981)
10. J.-H. Kim, J.C. Perez, W. Horton et al., Phys. Plasmas **13**, 062304 (2006)
11. D.D. Ryutov, Axisymmetric MHD-stable mirrors, in *Proceedings of Course and Workshop*, vol. II, Varenna, Italy, 791, 1987)
12. S. Migliuolo, Phys. Lett. A **131**, 373 (1988)
13. J.Y. Kim, W. Horton, D.I. Choi, S. Migliuolo, B. Coppi, Phys. Fluids B **4**, 152 (1992)
14. W.M. Tang, Nucl. Fus. **18**, 1089 (1978)
15. T. Cho et al., Phys. Rev. Lett. **97**, 005501-2 (2006)
16. T. Cho, J. Kohagura, M. Hirata et al., Nucl. Fus. **45**(12), 1656 (2005)
17. T. Cho, Private correspondence (Dec 24th, 2006)